Nonlinear Dynamics and Systems Theory, **22** (2) (2022) 178–196

Direct Torque Control of Three-Phase Induction Motor Powered by Three-Level Indirect Matrix Converter

Ameur Khaldi [1*], El Madjid Berkouk [1], Mohand Oulhadj Mahmoudi [1] and Abdellah Kouzou [2]

[1] *Process Control Laboratory, National Polytechnic School, Algiers, Algeria.*
[2] *Laboratory of Applied Automation and Industrial Diagnosis, Faculty of Sciences and Technology, Djelfa University, Algeria.*

Received: October 6, 2021; Revised: March 29, 2022

Abstract: In this paper, the three-phase induction machine (IM) fed by a three-level indirect matrix converter (IMC3) is proposed and investigated. Indeed, the IMC3 converter consists of a current rectifier connected to a three-level neutral-point-clamped voltage source inverter (NPC-VSI) without a bulky DC link capacitor interface. The rectifier ensures the bidirectional power transfer, where it is controlled by the space vector modulation (SVM) with the aim to obtain nearly a unity input power factor and to improve the input current waveform by the minimization of the harmonics content. On the other hand, the direct torque control (DTC) strategy is used to ensure the control of the three-phase IM, where the appropriate voltage vectors applied on the IM are generated via the control of the NPC-VSI. This combination can benefit from the advantages of the DTC and the IMC3 at the same time, allowing to improve the dynamic performances of the controlled three-phase IM compared to conventional topologies. For the validation of the advantages brought by this combination of the proposed topology of the used converter and the control strategy, simulations tests have been carried out.

Keywords: *direct torque control; induction machine; three-level inverter; space vector modulation; indirect matrix converter.*

Mathematics Subject Classification (2010): 70K70, 70K75, 34H05, 93B52, 93C10.

* Corresponding author: mailto:khaldi.ameur@gmail.com

1 Introduction

In the AC drive system, there are several converter topologies. The first family provides AC-DC conversion followed by DC - AC conversion. The main drawback of this converter is the use of a large capacitor on the DC link which has a limited lifetime when compared to the power devices, and increases the volume of the used converter. The second family ensures a direct conversion alternating-alternating (AC/AC). This direct conversion can be achieved either by cycloconverters or by matrix converters. The matrix converter is a recent topology of the frequency converters. This makes it possible to obtain an output voltage with variable amplitude and frequency from a fixed power supply voltage [1]. This can be achieved by the bidirectional current and voltage power switches, which are used in this kind of converters. Indeed, the matrix converter has many advantages such as

- A wide range of output frequency.
- The power factor at the output can vary freely according to the operating point of the load.
- The power factor at the input can be nearly unitary, and it can be imposed by the control.
- The operation in the four quadrants of the voltage-current plane.

However, it has some disadvantages such as

- The switching of current is more difficult due to the absence of the freewheeling diodes.
- The ratio of output-input voltage is reduced to 0.8666.

There are two topologies of matrix converters: the direct matrix converter (DMC) and indirect matrix converter (IMC).

The direct matrix converter (DMC) was first introduced by Gyugyi [2]. It connects directly three inputs to three output phases via nine bidirectional switches where basically the space vector modulation is used to ensure its control [3]. The conventional concept of space vector modulation (SVM), which was used for the control of inverter topologies, has been extended to ensure the control of the matrix converters with the aim to obtain improved input and output currents waveforms of the DMC [4].

In [5], the direct matrix converter is used with the direct torque control where a new switching table has been developed for this control taking into account the input displacement angle as a third control variable. On the other hand, the indirect matrix converter (IMC) scheme was firstly introduced by Huber and Borojevic [6]. It consists of a current rectifier connected to a voltage source inverter without intermediate bulky circuit [7]. The paper [8] investigates the application of the conventional DTC strategy for the induction machine based on the IMC. The classical DTC is based on the control of the inverter stage, where on the rectifier stage it is used to produce the DC bus voltage at the input side of the DC-AC stage, at the same time, it can be also controlled to ensure improved input current waveform and input power factor.

Indeed, to improve the quality of output voltage, the three-level indirect matrix converter (IMC3) was suggested and investigated by the authors in [9]. This topology is composed of a rectifier stage incorporated with a three-level-neutral point clamped voltage source inverter that has the ability to generate three-level voltages at the outputs.

In order to use the NPC VSI with IMC3 , the DC voltage provided by the rectifier V_{pn} is subdivided into two voltage levels V_{po} and V_{on} , and the neutral point (o) is connected to the star connected input filter capacitor as shown in Figure 1. To ensure balanced input capacitor voltages, the nearest three virtual space vector modulation (NTV SVM)

approach is used to control the DC-AC stage. This method requires that the sum of the three output phase currents equals zero at any sampling time.

In this paper, the application of a direct torque control based on the IMC3 to ensure the control of the three-phase induction motor is analyzed. It is well known that in the DTC, the generation of the control signals of the voltage source inverter switches depends on the output of the hysteresis comparators and the position of stator flux, which requires high frequency switching in the case of conventional two-level inverters. At the same time, when the conventional two-level inverter is used, the switches are subject to high voltage stress or high current when used in high voltage or high power application, respectively. However, the recent multilevel converter topologies (IMC3) seem to be well suitable for high voltage and high power applications, due to the segmentation of voltages and currents within the relatively high number of switches, hence they allow the use of fast semiconductors (eg. IGBT) where the commutation can be ensured as required without any risk or impact on the operational safety of the whole system. Based on these main advantages offered by the IMC3 topology and the direct torque control technique, the present paper investigates the use of the DTC with the IMC3 to ensure the control of the three-phase IM. Indeed, the high number of available voltage vectors resulting from the IMC3 and the use of the five-level torque controllers enhance considerably the output signal quality and the drive performances. It can be said initially that this combination of the DTC and IMC3 makes it possible to minimize the harmonics content of the output voltage and current, which have an important effect on the dynamic control of the IM.

The present paper is organized as follows. Section 2 introduces the modeling of induction machine, whereas Section 3 presents the DTC principle. The three-level neutral-point-clamped voltage source inverter is explained in Section 4. In Section 5, the DTC based on the IMC3 is presented, whereas simulation results are presented in the last section for the validation of the proposed control strategy. Finally, a conclusion is presented at the end of the paper.

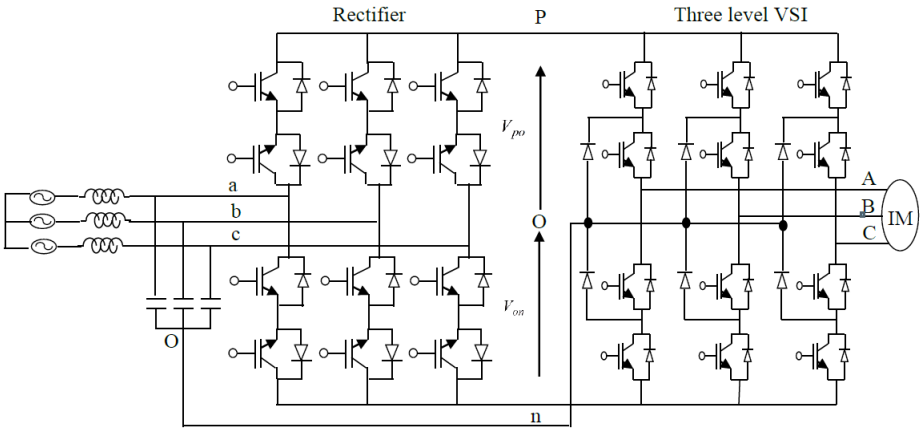

Figure 1: Three-level indirect matrix converter.

2 Modeling of Induction Machine

The induction machine consists of a stator which is connected to the power supply or a variable-speed drive and a short circuited rotor [10]. The model of the induction motor is presented in $(\alpha\beta)$ as follows:

$$V_s = R_s I_s + \frac{d\varphi_s}{dt}, \tag{1}$$

$$V_r = R_r I_r + \frac{d\varphi_r}{dt}. \tag{2}$$

V_s is the stator voltage and V_r is the rotor voltage, I_s is the stator current and I_r is the rotor current. Here

$$\varphi_s = L_s I_s + L_m I_r, \tag{3}$$

$$\varphi_r = L_r I_r + L_m I_s. \tag{4}$$

φ_s is the stator flux and φ_r is the rotor flux, L_s, L_r are the stator and rotor self-inductances, L_m is the mutual inductance.

The electromagnetic torque equation developed by the motor is expressed as follows:

$$T_{em} = \frac{3}{2} p \frac{L_m}{\sigma L_s L_r} \varphi_s \varphi_r \sin\theta, \tag{5}$$

σ is the leakage factor, p is the number of pole pairs and θ is the torque angle.

The equation of motion, connecting the electrical and mechanical parts, is written as follows:

$$j\frac{d\Omega}{dt} = T_{em} - T_r(\Omega). \tag{6}$$

T_{em} and T_r are the electromagnetic torque and the load torque, j is the rotor inertia.

3 Direct Torque Control Principle

The direct torque control (DTC) technique was proposed by Isao Takahashi in 1986 [11]. It consists of a pair of hysteresis controllers, a flux and torque estimators, and a voltage vector selection table. The basic advantages of the DTC scheme are presented as follows:

- High dynamic.
- Robustness.
- Reduced response time.
- Absence of park transformation.

The DTC has also some disadvantages, namely, the control of the torque and the flux at low speed is difficult, the switching frequency is not constant. The last one produces higher current and torque ripple and, consequently, higher machine losses, more noises and mechanical stress, which may reduce the lifespan of the machine. It is well known that the direct torque control (DTC) of an induction machine is based on the "direct" determination of the sequence of the control signal applied to the switches of the used voltage source inverter. This choice is generally based on the use of hysteresis regulators whose function is to control the amplitude of the stator flux and the electromagnetic torque. In Figure 2(a) and Figure 2(b) the schematic circuit of the conventional three-phase two-level voltage source inverter and the voltage vectors corresponding to the eight different possible switching configurations are presented, where two vectors determine the zero voltage vectors V_0 and V_7.

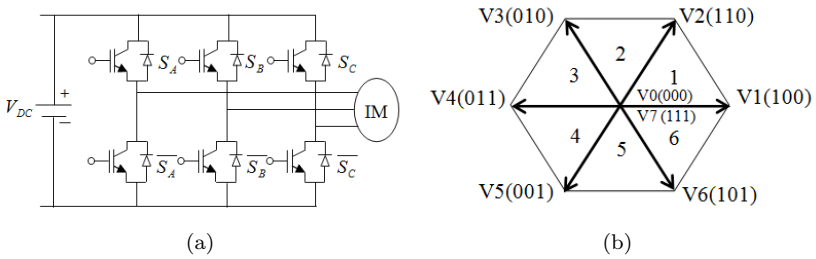

(a) (b)

Figure 2: (a) Schematic circuit of voltage source inverter, (b) Switching configurations of voltage vectors.

3.1 Stator flux control

The stator voltage in the stationary reference frame ($\alpha\beta$) of the three-phase IM can be obtained as follows:

$$V_s = R_s I_s + \frac{d\varphi_s}{dt}. \tag{7}$$

Hence, the stator flux can be expressed as

$$\varphi_s = \varphi_{s0} + \int_0^t (V_s - R_s I_s) dt. \tag{8}$$

Neglecting the voltage drop due to the stator resistance, the stator flux can be written as follows:

$$\varphi_s = \varphi_{s0} + \int_0^t (V_s) dt. \tag{9}$$

It can be considered that during a sampling period T_s, which is usually infinitesimal, the voltage vector applied to the IM remains constant, therefore

$$\varphi_s(k+1) = \varphi_s(k) + V_s T_s \rightarrow \Delta\varphi_s \simeq V_s T_s. \tag{10}$$

T_s : Sampling period,
$\varphi_s(k+1)$: Stator flux vector at the next sampling period $(k+1)T_s$,
$\varphi_s(k)$: Stator flux vector at current sampling period kT_s,
$\Delta\varphi_s$: Flux variation vector$(\varphi_s(k+1) - \varphi_s(k))$.

While the sampling period is fixed, $\Delta\varphi_s$ is proportional to the voltage vector applied to the motor.

From the equation (10), it is clear that the vector flux φ_s can be perfectly controlled by the voltage vector V_s.

3.2 Torque control

The torque equation is expressed as follows:

$$T_{em} = \frac{3}{2} p \frac{L_m}{\sigma L_s L_r} \varphi_s \varphi_r \sin\theta, \tag{11}$$

where θ is the torque angle which represents the shift angle between the flux vectors φ_s and φ_r (relative position of flux vectors).

It is obvious from equation (11) that the torque depends on the flux vectors φ_s and φ_r and on their relative position θ. However, the amplitude of φ_s is kept limited in the hysteresis band around its reference value and the amplitude of φ_r is also approximately constant. Consequently, the electromagnetic torque depends only on the angle (θ), which means that T_{em} increases with the increase of θ, and T_{em} decreases when θ decreases. The error between the reference flux and the estimated flux is introduced into the hysteresis controller which generates a variable C_φ. When $C_\varphi = 1$, it means that the amplitude of the flux should be increased, whereas when $C_\varphi = -1$, it means that the amplitude of the flux should be decreased. On the other hand, the error between the reference torque and the estimated torque is processed by a three-level hysteresis controller which generates the variable C_T which may take three values 1,-1 and 0. When $C_T = 1$, it means that the amplitude should be increased, and when $C_T = -1$, it means that it should be decreased. If $C_T = 0$, then it should be kept constant. Table 1. shows the different voltage vectors to be applied in order to maintain the stator flux and the electromagnetic torque inside their hysteresis bands.

C_φ	1	1	1	-1	-1	-1
C_T	1	0	-1	1	0	-1
$S(1)$	V_2	V_7	V_6	V_3	V_0	V_5
$S(2)$	V_3	V_0	V_1	V_4	V_7	V_6
$S(3)$	V_4	V_7	V_2	V_5	V_0	V_1
$S(4)$	V_5	V_0	V_3	V_6	V_7	V_2
$S(5)$	V_6	V_7	V_4	V_1	V_0	V_3
$S(6)$	V_1	V_0	V_5	V_2	V_7	V_4

Table 1: The basic DTC switching table using VSI.

As an example, if the stator flux vector is in the first sector, the voltage vectors V_2 and V_6 can be applied to increase the flux, whereas, the vectors V_3 and V_5 can be selected to decrease the flux. On the other hand, within the same sector, the vectors V_2 and V_3 can be used to increase the torque and the vectors V_5 and V_6 can be applied to decrease the torque. A general block diagram of the DTC scheme is presented in Figure 3.

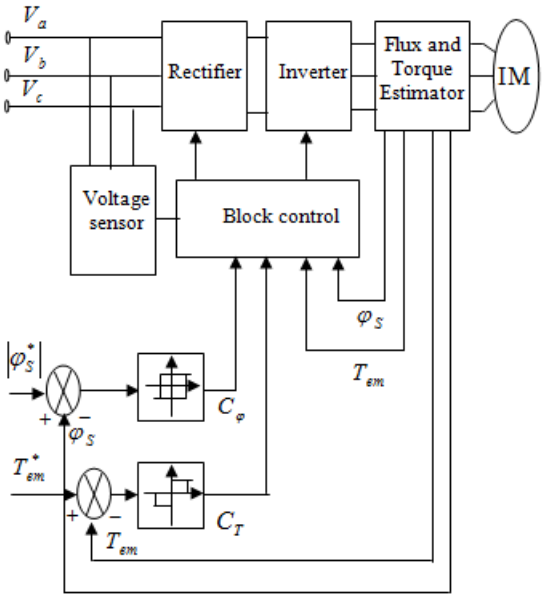

Figure 3: Block diagram of the DTC.

4 Three-Level Neutral-Point-Clamped Voltage Source Inverter

The neutral-point-clamped (NPC) inverter has many advantages [12, 13]. The voltage across each semiconductor is halved, which reduces the voltage stress, the harmonic content of the output voltages is diminished compared to the conventional two-level inverter. However, the capacitor voltage unbalance at the input side of the inverter increases the voltage stresses on the semiconductors and leads to the distortion of the output voltage [14, 15]. Furthermore, they may be subject to the voltage unbalance, which causes the unbalance of the three-phase output voltages. In this topology, in each phase/leg, there are 4 switching devices and 6 diodes that allow performing a combination of 27 switching states (Figure 4(a)).

It is obvious that the switching states can be presented by space voltage vectors. This representation is illustrated in Figure 4(b).

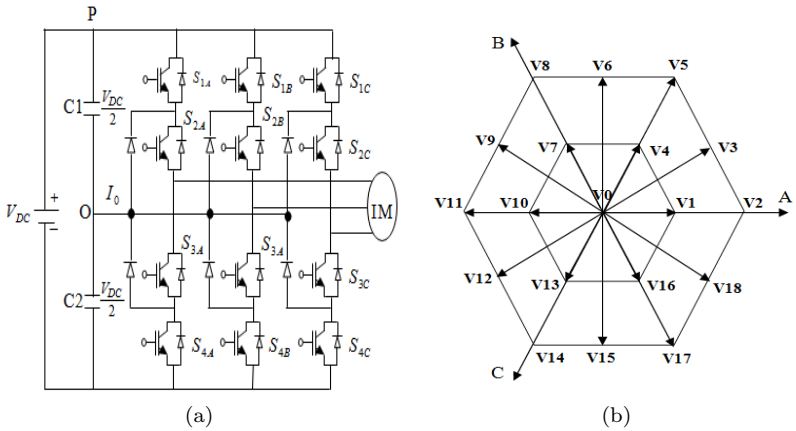

(a) (b)

Figure 4: (a) Three-level neutral-point-clamped voltage source inverter, (b) Space vector diagram of three-level inverter.

According to the possible switching states that may be achieved for each leg following the combination presented in Table 2, it is clear that there are three possible voltage levels: $\frac{V_{DC}}{2}, 0, \frac{-V_{DC}}{2}$. These values justify the ability of the presented topology to generate three-level outputs voltage. The space voltage vectors can be divided into four groups:

S_{1x}	S_{2x}	S_{3x}	S_{4x}	$V_{x0} : x \in \{A, B, C\}$	Switching states
ON	ON	OFF	OFF	$\frac{V_{DC}}{2}$	P
OFF	ON	ON	OFF	0	0
OFF	OFF	ON	ON	$\frac{-V_{DC}}{2}$	N

Table 2: The switch combination of three-level NPC VSI.

the zero vectors group, the small vectors group, the medium vectors group and the large vectors group as shown in Figure 4(b) [16].

5 DTC Based on Three-Level Indirect Matrix Converter

The three-level indirect matrix converter consists of a current rectifier connected to a three-level neutral-point-clamped voltage source inverter. The rectification stage has nine allowed combinations, it is formed by a six bidirectional switches so that the three-level indirect matrix converter can operate in the four quadrants. In this stage, the positive input voltage is connected to the p-terminal and the negative input voltage is connected to the n-terminal of the DC bus to generate the DC link voltage at the input side of the inverter stage. The NPC-VSI has nineteen voltage vectors describing 27 possible switching states, where three switching states among them produce the zero vector. This zero vector allows avoiding the DC bus short circuit and the open circuits in the case of inductive load which is the case of the IM. The other vectors are divided into three groups such as the large vectors (six vectors corresponding to six switching

states), medium vectors (six vectors corresponding to six switching states) and small vectors (six double vectors corresponding to twelve switching states). All of these vectors (large, medium, small and zero) are exploited to improve the control of the three-phase IM performances. As aforementioned, in this paper the advantages of the DTC and the IMC3 are combined to improve the performances of the control of the three-phase IM such as the response time, the precision of the developed torque and allowing the operation in the four quadrants of the torque-speed plane. Thus, a switching table is issued based on this combination which allows the generation of the appropriate vectors to be applied to the induction machine via the NPC-VSI [17].

5.1 The rectifier side control

In the rectification stage, only the two largest line-to-line input voltages in every sector are used. For example, in the first sector, the two maximum voltages u_{ac} and u_{ab} are considered as the supply for the inverter stage. The rectifier stage is controlled by a traditional space vector modulation. This method is based on [18]:

- the determination of the sector where the current or voltage reference is located;
- the application of the nearest vectors;
- the calculation of the corresponding duty cycles.

The input voltage vector can be represented as follows:

$$V_i = \frac{2}{3}(V_a + aV_b + a^2V_c), \tag{12}$$

where $a = \mathrm{e}^{j\frac{2\pi}{3}}$, V_i is the input voltage vector, V_a, V_b and V_c are the three phase-input voltages. The reference input current space vector can be represented as follows:

$$\bar{I_{in}} = I_{im}\mathrm{e}^{(j\omega_i - \varphi_i)} = I_{im}\angle\theta_i, \tag{13}$$

I_{im} is the magnitude of the reference vector, ω_i is the angle of the input voltages, φ_i is the displacement angle between the fundamental of input current phase and the corresponding line-to-neutral voltage, $\theta_i = \omega_i - \varphi_i$ is the direction of reference vector.

There are six active current space vectors, as shown in Figure 5(a). Each one represents the connection of the input phase voltages to the terminals of the DC-link. For example, the current $I_5 = (c, b)$ vector represents the connection of the input phase voltage V_c to the p-terminal and V_b to the n-terminal. The reference current vector can be synthesized with the two adjacent vectors (I_v, I_u) as shown in Figure 5(b).

The corresponding duty cycles are

$$d_u = \frac{T_u}{T_s} = m_R \sin(\frac{\pi}{3} - \theta_i), \tag{14}$$

$$d_v = \frac{T_v}{T_s} = m_R \sin(\theta_i), \tag{15}$$

$$d_0 = \frac{T_0}{T_s} = 1 - d_u - d_v. \tag{16}$$

The zero current vector cannot be used, so the duty cycles of rectification stage are adjusted as follows:

$$d_u^R = \frac{d_u}{d_u + d_v}, \tag{17}$$

$$d_v^R = \frac{d_v}{d_v + d_u}. \tag{18}$$

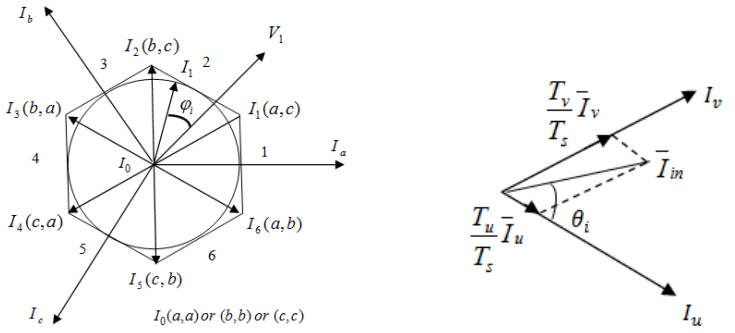

(a) (b)

Figure 5: (a) Input voltage and current vectors, (b) Generation of the reference input current.

5.2 The three-level inverter side control

The three-level inverter of the IMC3 ensures more control flexibility by offering several choices for the selection of the voltage vector under the direct torque control. Indeed, a switching table of the control structure makes it possible to select the appropriate voltage vector at each sampling instant according to the state of the flux and torque comparators and the sector where the stator flux vector is located [19–22]. The chosen vector should satisfy the requirement of the torque and the flux, and limits ΔV voltage to $\frac{V_{DC}}{2}$.

For instance, suppose that the stator flux is located in the first sector, and the currently used voltage vector is V_2 . To increase the torque and the flux, V_5 should be selected. In this case, a high $\frac{\Delta V}{dt}$ is applied on the semiconductor of the phase B, which should be avoided. However, this problem can be resolved by inserting a medium voltage vectors, which leads to reducing considerably the voltage stress across these devices. The position of the stator flux can be calculated as follows:

$$\theta_s = \arctan \frac{\varphi_{\beta s}}{\varphi_{\alpha s}}, \tag{19}$$

$\varphi_{\alpha s}$ and $\varphi_{\beta s}$ are the components of the stator flux in $\alpha\beta$ reference axes.

The reference torque can be obtained at the output of a PI which receives at its input the speed which presents the difference between the reference speed and the machine rotor speed. This reference torque is compared with the estimated value, and the error is processed using five-level hysteresis comparator which allows minimizing the torque ripples and improving the dynamic behavior of the electromagnetic torque developed by the machine.

The error ($\varepsilon_T = T^*_{em} - T_{em}$) belongs to one of the five regions fixed by the following constraints:
$C_T = +2$ for ($\epsilon_{Tmax2} < \epsilon_T$) high increase,
$C_T = +1$ for ($\epsilon_{Tmax1} < \epsilon_T < \epsilon_{Tmax2}$) small increase,
$C_T = 0$ for ($\varepsilon_{Tmin1} < \varepsilon_T < \varepsilon_{Tmax1}$) maintaining,
$C_T = -1$ for ($\varepsilon_{Tmin2} < \varepsilon_T < \varepsilon_{Tmin1}$) small decrease,
$C_T = -2$ for ($\varepsilon_T < \varepsilon_{Tmin2}$) high decrease,

$\varepsilon_{Tmax2} = 0.1$, $\varepsilon_{Tmin2} = -0.1$, $\varepsilon_{Tmax1} = 0.04$, $\varepsilon_{Tmin1} = -0.04$.

The estimated flux is compared with its reference value and the error is introduced to a three-level hysteresis controller. The error ($\varepsilon_\varphi = \varphi_s^* - \varphi_s$) is located in one of three regions defined by the following constraints:
$C_\varphi = +1$ for $\varepsilon_\varphi > \varepsilon_{\varphi max}$,
$C_\varphi = 0$ for $\varepsilon_{\varphi min} > \varepsilon_\varphi > \varepsilon_{\varphi max}$,
$C_\varphi = -1$ for $\varepsilon_\varphi < \varepsilon_{\varphi min}$,
$\varepsilon_{\varphi max} = 0.001$, $\varepsilon_{\varphi min} = -0.001$.

The three-level torque controller and the five-level flux controller are shown in Figure 6(a) and Figure 6(b) According to the flux and torque errors and the position of the

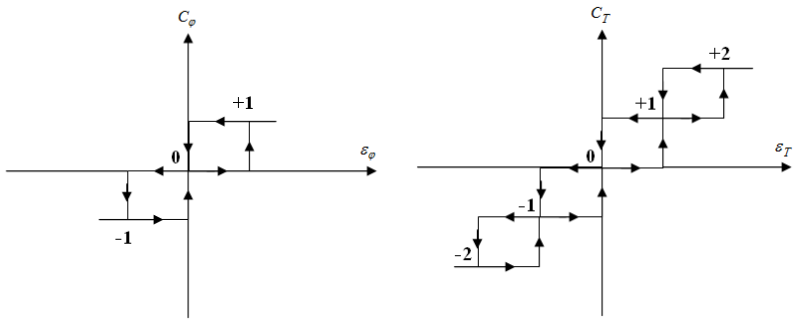

(a) (b)

Figure 6: (a) Flux hysteresis comparator, (b) Torque hysteresis comparator.

stator flux, an appropriate voltage vector from the 19 vectors generated by the NPC inverter is selected to maintain the flux and torque within the limits of hysteresis bands. Assume that the stator flux is located in the first sector to increase the flux.
For a large increase of the torque, the vector V_5 is used to diminish the torque and the flux errors. During one T_s , φ_s advances by the angle (δ_1) from its last position and therefore, the corresponding angular speed (ω_{s1}) is expressed as follows (Figure 7(a)) : $\omega_{s1} = \dfrac{\delta_1}{T_s}$. Consequently, the new formed angle between the stator and rotor flux becomes equal to $\theta + \delta_1$, which results in a large increase of the torque compared to its last value, whereas the rotor flux continues rotating by (ω_{s1}). For a small increase of the torque, the vector V_3 is applied. The stator flux advances by angle δ_2, regarding that $\delta_2 < \delta_1$. The angular speed (ω_{s2}) is given as follows (Figure 7(b)): $\omega_{s2} = \dfrac{\delta_2}{T_s} < \omega_{s1}$.

The rotation speed of the stator flux is reduced compared to its previous value. This leads to reducing the angle between φ_s and φ_r, which therefore leads to a small increase of the torque [23–27]. A voltage vector is generated (Table 3) depending on the position of the stator flux and the output of the two comparators.

6 Simulation Results

For the validation of the application of the proposed control on the three-level indirect matrix converter topology driving a three-phase induction motor, two simulation tests

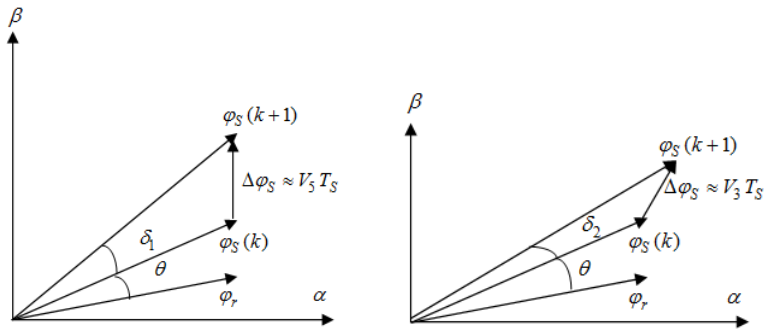

(a) (b)

Figure 7: (a),(b) Evolution of the flux vector in the $\alpha\beta$ plane.

C_φ	C_T	$S(1)$	$S(2)$	$S(3)$	$S(4)$	$S(5)$	$S(6)$
+1	+2	V_5	V_8	V_{11}	V_{14}	V_{17}	V_2
+1	+1	V_3	V_6	V_9	V_{12}	V_{15}	V_{18}
+1	0	V_0	V_0	V_0	V_0	V_0	V_0
+ 1	-1	V_{18}	V_3	V_6	V_9	V_{12}	V_{15}
+1	-2	V_{17}	V_2	V_5	V_8	V_{11}	V_{14}
0	+2	V_4	V_7	V_{10}	V_{13}	V_{16}	V_1
0	+1	V_4	V_7	V_{10}	V_{13}	V_{16}	V_1
0	0	V_0	V_0	V_0	V_0	V_0	V_0
0	-1	V_0	V_0	V_0	V_0	V_0	V_0
0	-2	V_{13}	V_{16}	V_1	V_4	V_7	V_{10}
-1	+2	V_8	V_{11}	V_{14}	V_{17}	V_2	V_5
-1	+1	V_9	V_{12}	V_{15}	V_{18}	V_3	V_6
-1	0	V_0	V_0	V_0	V_0	V_0	V_0
-1	-1	V_{12}	V_{15}	V_{18}	V_3	V_6	V_9
-1	-2	V_{14}	V_{17}	V_2	V_5	V_8	V_{11}

Table 3: The basic DTC switching table using VSI.

have been carried out under normal speed with sudden rotation reversal and under low speed with sudden rotation reversal. The input of the matrix converter is connected to three-phase 220V, 50HZ power supply and the induction motor to be controlled is of power 1.5kW and its parameters are presented in Table 4.

6.1 Scenario 1

In this scenario, the profile of the reference speed is presented in Figure 8(a), where the speed is the same for the forward and backward rotation with a value of 100 rad/s and -100 rad/s, respectively. It can be seen clearly that the motor follows the reference profile precisely without any kind of overshoot after short transient durations along the start-up and the sudden rotations reversal, which last 0.32s and 0.40s, respectively, as

Rated power	1.5 kw
Rated current	3.7 A
Rated speed	1420 r/m
Rated Torque	10 N.m
Number of pole pairs	2
Stator resistance	4.85 Ω
Rotor resistance	3.805 Ω
Stator self inductance	0.274 H
Rotor self inductance	0.274 H
Mutual inductance	0.285 H
Rotor inertia	$0.031 kg.m^2$
Friction coefficient	$0.001136 N.m.s/rd$

Table 4: The induction machine parameters.

shown in Figure 8(a). Indeed, the mismatch between the reference speed and the motor rotor speed at steady state is nearly neglected, which proves that the applied control on the studied topology fulfills the requirements of the speed imposed at relatively normal speed values. On the other hand, to check the robustness of the speed control under torque load changes, a load torque is applied into two intervals of $t \in [0.6s, 0.9s]$ and $t \in [2s, 2.2s]$ with a value of 5N.m and -5N.m, respectively. It can be seen clearly that the changes of the load torque have no impact on the speed where it remains equal to the reference speed, which proves the robustness of the applied control on the studied topology in terms of load torque variation within the rated values of the motor.

Figure 8(b) represents the dynamic response of the electromagnetic torque developed by the motor T_{em} to ensure the dynamics of the motor imposed by the speed profile and the applied load torque. It can be noted that during the startup step at no load, the motor operates at the acceleration mode to reach the imposed reference speed, and therefore, T_{em} should behave accordingly where it takes the value of 10N.m to ensure a fast passage of such mode, whereas when the rotor speed reaches the reference speed at $t = 0.32s$, T_{em} falls to the value of 0.11N.m, which is equal to the value of torque resulting from the motor friction. When the load torque $T_L = 5N.m$ is applied to the induction machine shaft during the time interval $t \in [0.6s, 0.9s]$, the T_{em} is changed accordingly to be equal to the load torque. The zoom window taken at this time interval proves clearly the high dynamics of T_{em} as shown in Figure 8(b), where its average value is slightly greater than the load torque, this is due to the fact that the resulting friction torque aforementioned is added to the load torque. The same dynamics behavior of the T_{em} can be observed in the zoom window within the time interval $t \in [2s, 2.2s]$ when the motor is running in the backward direction with the same speed of -100 rad/s and the load torque $T_L = -5N.m$ as shown in Figure 8(b). It is worthy to clarify the high dynamics of the used control during the rotation reversal of the machine at time 1.3s, where the electromagnetic torque increases promptly to -10N.m in the inverse direction to ensure the inversion of the rotor speed which is achieved nearly within 0.4s passing through the deceleration mode during $t \in [1.2s, 1.4s]$ and the acceleration mode in the backward direction during $t \in [1.4s, 1.6s]$. As the rotor speed of the machine reaches the reference speed -100 rad/s, the electromagnetic torque is set back to be equal to

the resulting machine friction torque as shown in Figure 8(b). Based on the whole observation of Figures 8(a) and 8(b), it can be said that the used control with the used inverter topology allow ensuring a high dynamics performance control of the machine with an accurate tracking of the reference speed and the load torque variations.

Figure 8(c) shows the stator flux which tracks the reference flux with a neglected deviation of 0.1% , where it keeps its value constant with a very neglected ripples along the variation of the speed and the load torque as it can be seen in the zoom windows taken at different intervals. Whereas the flux in the $(\alpha\beta)$ frame is shown in Figure 8(d), it presents a circle with a very tiny thickness.

The stator currents in the three phases are shown in Figure 8(e). Without taking into account the very short transient periods at different stage of start-up and speed reversal, it can be observed clearly within the zoom windows that the current is balanced under no-load and load torque application in both speed directions, where the measured currents are 1.48 A and 2.26 A, respectively. On the other hand, despite the output voltages of the matrix converter which are applied to the terminals of the machine, the currents absorbed by the machine possess sine waveform with neglected ripples as shown clearly within the zoom windows of Figure 8(e).

Figure 8(f) shows the DC-link voltage. It is obvious that it presents important fluctuations around its average value of 475 V. The zoom windows taken at four regions with a width corresponding to the power supply period of 0.02 s, demonstrate that the DC-link voltage fluctuates with a frequency which equals six times the frequency of the input voltage and its amplitude is limited within the range of 540 V and 310 V.

Figure 8(g) shows the IMC3 input current of phase "a", where it can be noted in each zoomed window at different intervals of time that this current is rich in harmonics and can be a source of pollution to the power supply. Therefore, a passive LC low pass filter is inserted between the source and the IMC3 input to reduce the harmonics content and to overcome this major problem. The resulting current at the power supply side of phase "a" is depicted in Figure 8(h), it can be seen clearly within the zoomed window in this figure that the power supply current has nearly a sine waveform, furthermore, the shift phase with the power supply voltage is zero, which means a nearly power factor is ensured. Therein, the zoomed window is within the interval of time $[1.2s, 1.8s]$ that presents the step of speed reverse, where the motor works into quadrant II and quadrant III. Indeed, in the quadrant II, the mode of operation is referred to the breaking of the motor to reach the zero speed, which means that the power absorbed from the source decreases and transfer of power is directed from the motor to the DC-link. Whereas, when the motor starts changing its speed, it works in the quadrant III and the power is transferred from the power supply to the motor, hence the current increases till it reaches the required value which is corresponding to the steady state speed. Based on the obtained simulation results, it can be concluded that the proposed control with the proposed topology of the IMC3 can ensure sufficient dynamics for the control of the speed of the motor under different aforementioned operation modes. It is also worthy to mention that the use of the multi-level IMC allows obtaining better flexibility of the control and avoiding the bulky topology of the conventional two-stage three-level inverter and its intermediate DC-link.

6.2 Scenario 2

In this scenario, the profile of the reference speed is presented in Figure 9(a). The motor operates along three modes. The first mode is the forward mode at low speed

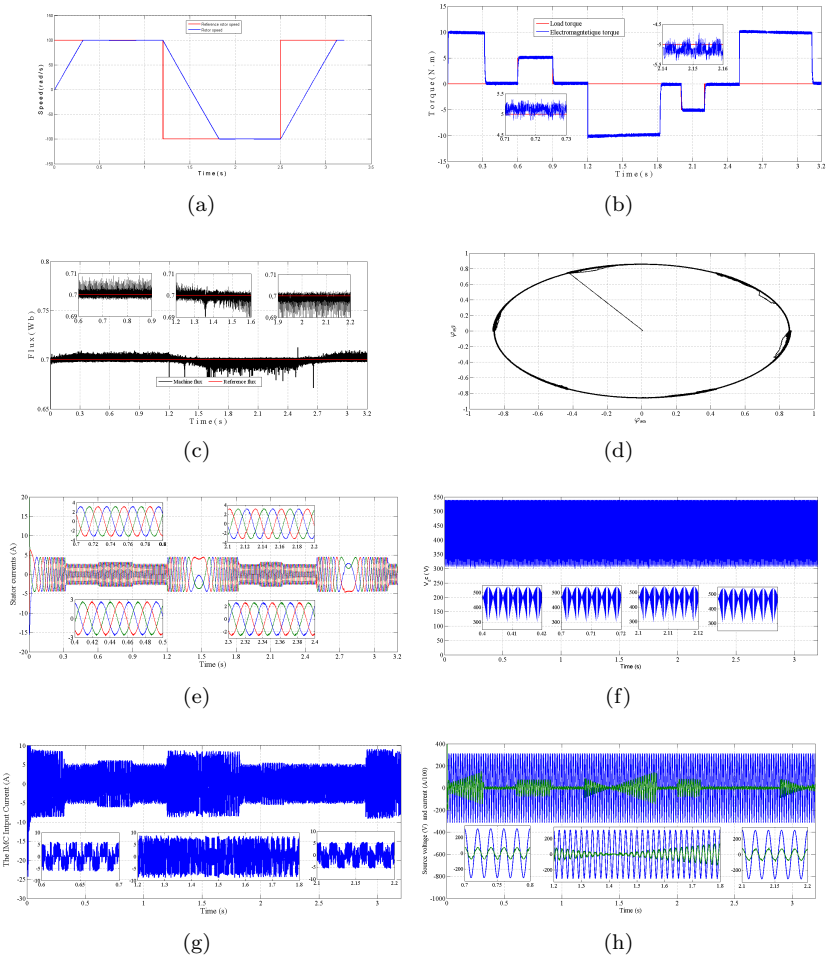

Figure 8: (a) The rotor speed of the controlled machine and the imposed reference speed, (b) The electromagnetic torque of the motor and the applied load torque, (c) The stator flux and the reference flux, (d) The stator flux in the ($\alpha\beta$) frame, (e) The stator currents, (f) The virtual DC-link between the rectifier stage and the three-level inverter stage in the used indirect matrix converter, (g) The input current of the IMC at phase "a", (h) The current and the voltage of phase "a" at the source side.

$t \in [0s, 1.2s]$, where the motor starts up from zero speed to reach its steady value of 30 rad/s. The second mode is the backward mode at low speed $t \in [1.2s, 2.5s]$, where the rotor speed is reversed to reach the steady value of -30 rad/s. The last mode is the forward mode at high speed $t \in [2.5s, 4s]$, where the rotor speed is reversed once more to reach the speed value of 100 rad/s. It can be noted clearly within the three steps of speed changes that the motor follows the reference profile precisely without any kind of overshoot after short transient durations along the start-up and the two sudden rotation reversals, which last 0.1s, 0.2s and 0.5s, respectively, as shown in Figure 9(a). On the other hand, a load torque is applied within two intervals of $t \in [0.6s, 0.9s]$ and

$t \in [2s, 2.2s]$ with a value of 5N.m and -5N.m, respectively, as shown in Figure 9(b). It can be noted that during the startup step at no load in the first mode and during the speed reversal in the third mode, the T_{em} takes the value of 10N.m to ensure a fast passage to the steady speed, whereas when the rotor speed reaches the reference speed, T_{em} falls to the value of the 0.034N.m, which is equal to the value of torque resulting from the motor friction. On the contrary, when the motor runs at steady speed in the two first modes, T_{em} is equal to the applied load torque during the time interval $t \in [0.6s\ ,\ 0.9s]$ and $t \in [2s, 2.2s]$ as shown in Figure 9(b) It is also observed that the electromagnetic torque increases according to the speeds changes to ensure the rapid tracking of the reference speed as shown in the different transition steps of the speed reference. Figure 9(c) shows the stator flux, where it is equal to the reference flux 0.7Wb with limited ripples. It can be seen clearly that when the speed is high, more ripples are observed, which is related to the increase of harmonics components magnitudes within the tolerable range. On the other hand, the motor currents change according to the transition steps and the applied load. It behaves similarly as in the first scenario, however the increase of current during the transition steps is less, as shown in Figure 9(d). The virtual DC-link voltage also behaves in the same way as in the first scenario with the same characteristics as shown in Figure 9(e). The source currents from the input side of the IMC3 before the filter have nearly a sine waveform and are in phase with the power supply voltage as it can be noticed for the phase "a" in Figure 9(f).

It can be concluded that the application of the DTC with the topology of three-level IMC can ensure improved performance dynamics for the control of the induction machine within a wide range of speed variation.

Based on the obtained results from the both investigated scenarios, it can be said that the presented topology of the three-level matrix converter presents better performance compared to the conventional two-level inverters, which are commonly used in many industrial applications. Indeed, the dynamic responses of the induction motor towards the variation of the load at nominal and low speed prove the improved reliability and the accuracy of the applied control technique with the aforementioned converter topology for ensuring the dynamic behavior of the induction motor. On the other hand, the used converter allows to provide a current with low harmonics content, which means low ripples in the developed torque, and hence less mechanical stresses are applied on the motor. At the same time, it is always possible to perform the control of the converter to meet the requirements of the quality of the input current, which is a major drawback within the conventional converter topologies, where the absorbed harmonics from the power source are minimized and their effect is limited. It is worthy to mention that based on the carried control, the input power factor is nearly equal to the unit, which means high efficiency of the whole system can be achieved.

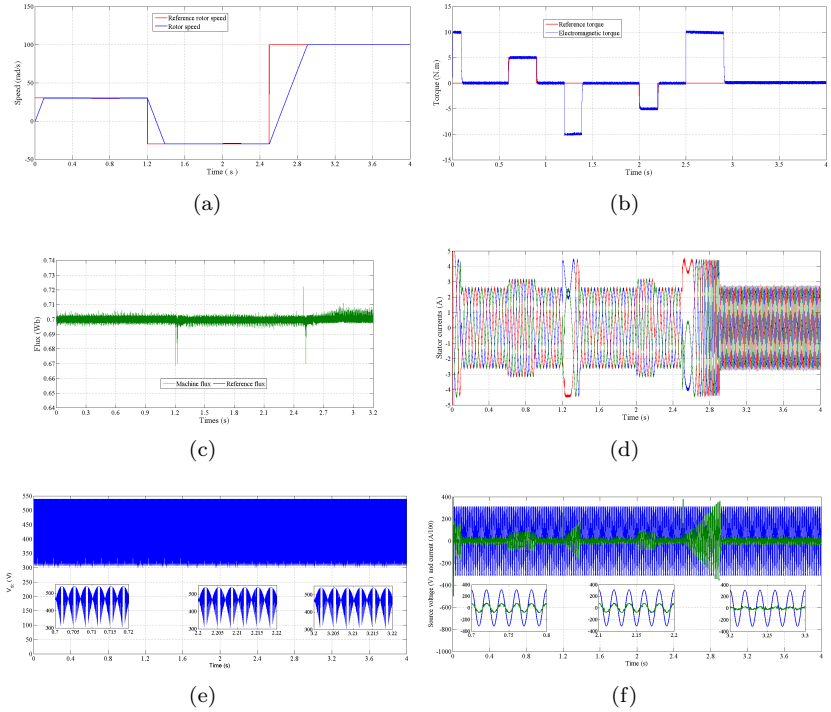

Figure 9: (a) The rotor speed of the controlled machine and the imposed reference speed, (b) The electromagnetic torque of the motor and the applied load torque, (c) The stator flux and the reference flux, (d) The stator currents, e) The virtual DC-link between the rectifier stage and the three-level inverter stage in the used indirect matrix converter, (f) current and the voltage of phase "a" at the source side.

7 Conclusion

In this paper, the direct torque control (DTC) technique is applied for the control of a three-phase induction machine within a wide speed range variation based on the use of a three-level indirect matrix converter (IMC3). The main aim of using the IMC3 under DTC technique is to ensure improved advantages compared to the conventional conversion topologies such as ensuring small size, eliminating the bulky DC-link, improving the output form, controlling the input current wave for controlling the input power factor, reducing the rate of $\frac{dV}{dt}$ at the used switches, and ensuring a fast and accurate torque response. Indeed, due to the large number of voltage vectors that can be generated by IMC3, the use of the IMC3 allows elaborating a switching table for the selection of the appropriate vectors to be applied to the induction machine to ensure the regulation of the stator flux and the electromagnetic torque with high performance, to improve the output current waveform to guarantee nearly sine waveform of the input current with unity power factor and to operate within a wide range of speed variation without deficiency. Based on the obtained simulation results, it can be said the application of the three-level indirect matrix converter for driving the three-phase induction motor can provide improved dynamic and static performances under an appropriate control technique such as

the DTC, in terms of dynamic responses, quality of input and output currents, range of speed variation, less ripples of torque, which lead to less vibrations and less mechanical constraints, less size and less costs.

References

[1] L. Neft and C. D. Shauder. Theory and design of a 30-hp matrix converter. *In: Conference Record. IEEE Industry Applications Society Annual Meeting* (October 1988) 934–939.

[2] B. Gyugyiand and Pelly. *Static Power Frequency Changer Theory. Performance and Application.* New York, Wiley–Interscience, 1976.

[3] D. Casadei, G. Grandi, G. Serra, and A. Tani. Space vector control of matrix converters with unity input power factor and sinusoidal input/ output waveforms. In: *European Conference on Power Electronics and Applications. IET* (1993) 170–175.

[4] L. Huber and D. Borojevic. Space vector modulator for forced commutated cycloconverters. In: *Conference Record of the IEEE Industry Applications Society Annual Meeting*, (October 1989) 871–876.

[5] D. Casadei, G. Serra and A. Tani. The Use of Matrix Converters in Direct Torque Control of Induction Machines. *IIEEE Transactions on Industrial Electronics* **48** (6) (2001) 1057–1064.

[6] L. Huber and D. Borojevic. Space Vector Modulated Three Phase To Three Phase Matrix Converter With Input Power Factor Correction. *IEEE Transactions on Industry Applications* **31** (6) (1995) 1234–1246.

[7] L. Huber, D. Borojevic. Space vector modulation with unity input power factor for forced commutated cycloconverters. In: *Conference Record of the IEEE Industry Applications Society Annual Meeting*, (1991) 1032–1041.

[8] X. Chen and M. Kazerani. A New Direct Torque Control Strategy for Induction Machine Based on Indirect Matrix Converter. *IEEE International Symposium on Industrial Electronics* **3** (2006) 2479–2484.

[9] MY. Lee, P. Wheeler and C. Klumpner. *new modulation method for the three-level-output-stage matrix converter. IEEE Power Conversion Conference* (2007) 776-–783.

[10] G. R. Slemon. Modeling of induction machines for electric drives. *IEEE Trans. Ind. Appl.* **25** (6) (1989) 1126-–1131.

[11] I. Takahashi and T. Noguchi. A new quick-response and high-efficiency control strategy of an induction motor. *IEEE Trans Ind Appl.* (1986) 820—827.

[12] N. Celanovic and D. Boroyevich. A comprehensive study of neutral-point voltage balancing problem in three level neutral-point-clamped voltage source PWM inverters. *IEEE Applied Power Electronics Conference* (1999).

[13] C. Yiqiang, M. Bakari, W. Zbigniew and O. Boonteck. Regulating and equalizing DC capacitance voltages in multilevel statcom. *IEEE Trans. on Power Delivery* (1997) 901–907.

[14] Jih-Sheng Lai and Fang Zheng Peng. Multilevel converters-a new breed of power converters. *IEEE Trans. Ind. Appl.* (1996) 509–517.

[15] A. Nabae, I. Takahashi and H. Akagi. A new neutral-point clamped PWM inverter. *IEEE Trans. Ind. Appl.* (1981) 518—523.

[16] C. Ui-Min and L. Kyo-Beum. Space vector modulation strategy for neutral-point voltage balancing in three-level inverter systems. *IET Power Electronics* (2013) 1390–1398.

[17] B. Chikondra, M. R . Utkal and B. K. Ranjan . Fault-tolerant dtc technique for five-phase three-level npc inverter-fed induction motor drive with an open-phase fault. *IEEE Energy Conversion Congress and Exposition (ECCE). IEEE* (2019).

[18] H. S. Purnama, HendrilSatrian, T. Sutikno and M. Facta. Modulation Strategies for Indirect Matrix Converter: Complexity, Quality and Performance. *5th International Conference on Electrical Engineering, Computer Science and Informatics (EECSI). IEEE* (2018).

[19] I. Messsaif, E. M. Berkouk and N. Saadia. Ripple reduction in DTC drives by using a three-level NPC VSI. *IEEE Trans. Ind. Appl.* (2007) 1179—1182.

[20] R. Zaimeddine, E. M. Berkouk, L. Refoufi and M. Bousalah. scheme of EDTC control using a three-level voltage source inverter for an induction motor. *The IEEE International Symposium on Industrial Electronics*. Vigo, Spain, 2007, 2250–2255.

[21] M. Bermudez, I. G. Prieto, F. Barrero, H. Guzman, M. J. Duran and X. Kestelyn. Open-phase fault-tolerant direct torque control technique for five-phase induction motor drives. *IEEE Tran. on Ind. Electron.* **64** (2) (2017) 902-–911.

[22] B. Ch, U. R. Muduli and R. K. Behera. Performance comparison of five-phase three-level npc to five-phase two-level voltage source inverter. In: *IEEE International Conference on Power Electronics, Drives and Energy Systems (PEDES)*, (December 2018) 1-–6.

[23] S. Payami, R. K. Behera and A. Iqbal. Dtc of three-level npcinverterfed five-phase induction motor drive with novel neutral point voltage balancing scheme. *IEEE Trans. on Power Electronics* **33** (2) (2018) 1487—1500.

[24] J. K. Pandit, M. V. Aware, R. V. Nemade and E. Levi. Direct Torque Control Scheme for a Six-Phase Induction Motor With Reduced Torque Ripple. *IEEE Trans. on Power Electronics* **32** (9) (2016) 7118–7129.

[25] I. M. Alsofyani and N. R. N. Idris. Simple Flux Regulation for Improving State Estimation at Very Low and Zero Speed of a Speed Sensorless Direct Torque Control of an Induction Motor. *IEEE Trans. on Power Electronics* **31** (4) (2015) 3027–3035.

[26] B. Chikondra, U. R. Muduli and R. Kumar Behera. Fault-Tolerant DTC Technique for Five-phase Three-Level NPC Inverter-fed Induction Motor Drive with an Open-Phase Fault. *IEEE Energy Conversion Congress and Exposition (ECCE)* (2019) 5281-–5287.

[27] P. Naganathan, S. Srinivas, and H. Ittamveettil. Five-level torque controller-based DTC method for a cascaded three-level inverter fed induction motor drive. *IET Power Electronics* (2017) 1223—1230.